

Time-domain Brillouin imaging of sound velocity and refractive index using automated angle scanning

Motonobu Tomoda^{a,*}, Akihisa Kubota^a, Osamu Matsuda^a, Yoshihiro Sugawara^b,
Oliver B. Wright^{c,d}

^a Faculty of Engineering, Hokkaido University, Sapporo 060-8628, Japan

^b Analysis Technology Center, FUJIFILM Corporation, Kanagawa 250-0193, Japan

^c Hokkaido University, Sapporo 060-0808, Japan

^d Graduate School of Engineering, Osaka University, Yamadaoka 2-1, Suita, Osaka 565-0871, Japan

ARTICLE INFO

Keywords:

Picosecond ultrasonics
Brillouin scattering
Time domain
Sound velocity
Refractive index
Ultrafast

ABSTRACT

We present a picosecond optoacoustic technique for mapping both the longitudinal sound velocity v and the refractive index n in solids by automated measurement at multiple probe incidence angles in time-domain Brillouin scattering. Using a fused silica sample with a deposited titanium film as an optoacoustic transducer, we map v and n in the depth direction. Applications include the imaging of sound velocity and refractive index distributions in three dimensions in inhomogeneous samples such as biological cells.

1. Introduction

Picosecond ultrasonics relies on the optical generation of acoustic stress by the absorption of ultrashort light pulses of sub-picosecond duration in opaque samples and the detection of propagating acoustic pulses by delayed light pulses through transient reflectance changes [1–3]. For the case of transparent samples coated with an opaque film, it is also possible to generate acoustic pulses thanks to the film optical absorption and to measure GHz Brillouin oscillations in optical reflectance arising from sound transmitted to the transparent medium [4–16]. The latter technique, known as picosecond ultrasonic interferometry or TDBS (Time-Domain Brillouin Scattering), relies on the photoelastic effect, and has been used for depth profiling and three-dimensional (3D) imaging of the longitudinal sound velocity in transparent samples, including biological cells, assuming a constant refractive index distribution [17–23]. In addition, various other applications have been suggested for TDBS, such as monitoring polycrystalline aggregates, ion implantation profiles, internal stress distributions, and temperature gradients [24–26]. TDBS has also been used to profile both the refractive index and sound velocity by multiple probe-light incidence angle measurements, but the proposed apparatus is not automated, leading to arduous data acquisition procedures [11,27,28].

In picosecond ultrasonics one makes use of a pump light beam, an

incident probe light beam, and a reflected/transmitted probe light beam, each associated with a focusing lens. To achieve small optical spots for optimal lateral resolution, lenses with a short focal length should be used. Space for separately positioned lenses is limited, so a single lens is often used for two or three beams. For example, when the probe beam is at normal incidence to the sample, a single lens focuses the incident probe beam to the sample and picks up the reflected probe beam. But in multi-angle measurement methods, more lenses are usually necessary, and result in crowded and complicated setups around the sample. For example, we previously reported a measurement involving a varying probe-beam incident angle using a θ - 2θ stage (as in an ellipsometer) with a hemispherical sample using a pick-up lens and detector mounted on a coaxial rotation stage [28]. Côte et al. also used a complicated sample-rotation setup for measurement with two probe incident angles [27]. Lomonosov et al. used three probe incident angles (0° , 45° , and 60°). All these multi-angle scan systems can only be efficiently used for samples which are laterally homogeneous because it is difficult to access exactly the same position on the sample at each probe incidence angle. Here we propose an experimental technique which allows the probe-incidence angle to be scanned with a simpler experimental setup, and extends TDBS to automated data acquisition suitable for spatially inhomogeneous samples. We make use of a single objective lens with a high numerical aperture for the pump, incident probe, and

* Corresponding author.

E-mail address: mtomoda@eng.hokudai.ac.jp (M. Tomoda).

<https://doi.org/10.1016/j.pacs.2023.100486>

Received 8 February 2023; Received in revised form 23 March 2023; Accepted 31 March 2023

Available online 11 April 2023

2213-5979/© 2023 The Authors. Published by Elsevier GmbH. This is an open access article under the CC BY-NC-ND license (<http://creativecommons.org/licenses/by-nc-nd/4.0/>).

reflected probe beams without the need for rotating the sample or adjusting the lens position.

2. Theory for mapping both sound velocity and refractive index in TDBS

Time-domain Brillouin oscillations measured with pulsed lasers arise from the interference between the probe light reflected from the acoustic pulse and from interfaces inside transparent samples. For homogeneous and isotropic samples, the Brillouin oscillation frequency f_B is given by

$$f_B = \frac{2nv\cos\theta}{\lambda}, \quad (1)$$

where n is the refractive index, v is the longitudinal sound velocity, θ is the probe incident angle on the plane normal to the propagation direction of the acoustic pulse, and λ is the wavelength of the probe light in vacuum. From the application of Snell's law, $n\sin\theta = \sin\theta_0$, at the sample surface, where θ_0 is the probe incident angle in air, Eq. (1) can be rewritten as follows:

$$f_B = \frac{2v\sqrt{n^2 - \sin^2\theta_0}}{\lambda}. \quad (2)$$

This is also valid when the sample is immersed in liquids using, for example, a liquid-immersion microscope objective.

By monitoring the time-resolved Brillouin oscillation frequency f_B as a function of multiple incident angles θ_0 and time allows one to obtain depth profiles of both v and n from Eq. (2).

3. Experimental setup with automated angle scanning

3.1. Automated angle scanning and sample description

The experimental method is based on conventional picosecond ultrasonics [1,2], making use of a pump optical beam to generate picosecond acoustic pulses and a delayed probe beam to detect their propagation. To enable probe-light incident angle scanning, we incorporate a microscope objective with a high numerical aperture (NA). Although high NA lenses are usually used for making small spots by the use of optical beams that fill a substantial fraction of the lens aperture, we use them here for a different aim. When a collimated narrow beam propagating parallel to the center axis of a microscope objective enters the objective at an in-plane lateral displacement defined by x and y from the lens axis, the incident angle θ_0 of the output beam on the focusing plane is given by

$$\theta_0 = \tan^{-1} \frac{\sqrt{x^2 + y^2}}{F}, \quad (3)$$

where F is the focal length of the microscope objective, as shown in Fig. 1(a). If we hold y at some fixed value close to zero while scanning x , it is therefore possible to vary the value of θ_0 . This is valid for output beams in air, but Eq. (2) also applies when the sample is immersed in a liquid. We use a water-immersion microscope objective (Olympus LUMPLFLN60XW), as shown by the image in Fig. 1(b), with NA = 1.0, $F = 3.0$ mm, working distance 2 mm, and lens aperture diameter 8 mm. To validate our technique, we choose an isotropic fused silica cover glass of thickness 0.3 mm (Sekiya Rika Co., Ltd, D14-081-010) coated on one side with an isotropic polycrystalline titanium film of thickness 640 nm made by RF (radio frequency) sputtering. The Ti film serves as an optoacoustic transducer based on thermoelastic expansion. A schematic of the sample is shown in Fig. 1(c). We choose Ti because it is known to be inert to living biological samples, and is commonly used in TDBS for such applications. The Ti thickness is chosen so that the round trip frequency of a longitudinal acoustic wave, ~ 4.8 GHz (period ~ 210 ps), calculated from the longitudinal sound velocity of Ti (6070 m s $^{-1}$ [29]) is significantly different from $f_B \sim 20$ GHz in the cover glass. The sample

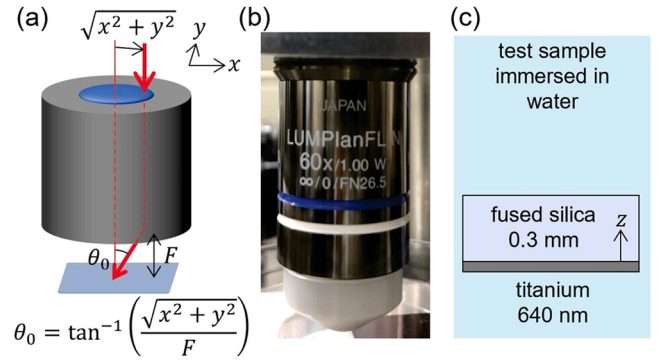


Fig. 1. (a) Schematic showing the relation between the incident off-axis displacement x and the output angle θ_0 of a narrow beam entering a microscope objective with focal length F . (b) Image of the water-immersion objective lens with numerical aperture NA = 1.0 (Olympus LUMPLFLN60XW). (c) Schematic showing the sample used.

and front end of the microscope objective are immersed in distilled water (refractive index $n = 1.33$, sound velocity 1482 m s $^{-1}$ [29]) in a Petri dish.

3.2. Measurement method

We make use of a mode-locked Ti:sapphire laser (center wavelength 820 nm, pulse width 200 fs, repetition frequency 80 MHz). A schematic diagram of the experimental system is shown in Fig. 2. A beam of near-infrared pulsed light of FWHM (full width half maximum) width ~ 1 mm before the objective lens is used as the probe light, and a frequency-doubled blue beam generated at a BBO (β -BaB $_2$ O $_4$) crystal is used as the pump light, of FWHM width ~ 2 mm before the objective lens, which generates longitudinal phonon pulses in the Ti film. The phonon pulses are transmitted to the silica cover glass, where they can scatter the probe light. The pump beam is chopped by an acousto-optic

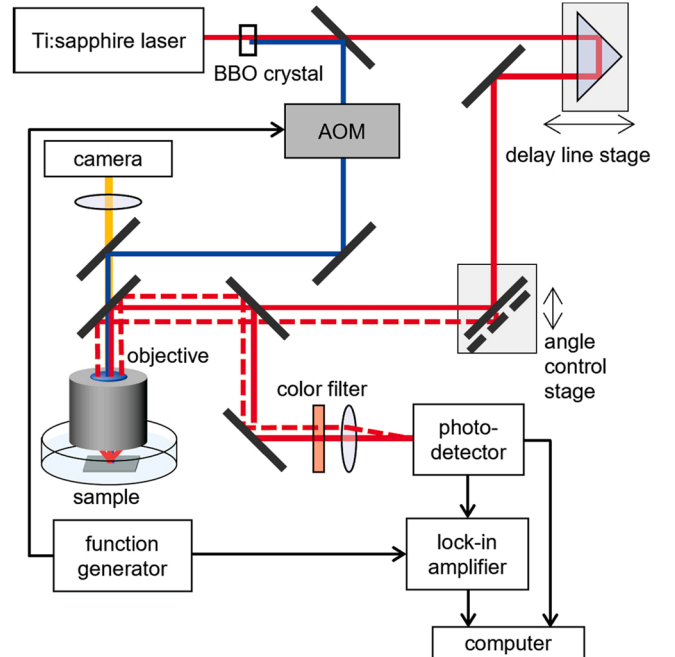


Fig. 2. Experimental setup. When the motorized angle control stage is linearly displaced by x for a fixed value of y , the probe beam and reflected probe beam entering and emerging from the objective are also displaced by x (dashed line). This displacement causes a change of the incident angle of the probe light on the sample. BBO: beta barium borate β -BaB $_2$ O $_4$, AOM: acousto-optic modulator.

modulator at 1 MHz and focused on the sample by the objective lens. The probe beam is collimated and shaped to ~ 1 mm diameter by a lens pair and an iris, and then passes through a delay line which consists of a motorized linear stage and a corner-cube reflector. The delayed probe beam is further guided to a mirror placed on another linear motorized stage (the angle-control stage). Here the 90° -reflected beam is variably displaced by the motion of the angle-control stage, as shown in Fig. 2. When this stage is displaced by x from the x origin, the probe beam path is laterally displaced by the same amount without changing the beam propagation direction. In this way, the position of the incident beam with respect to the objective is also moved by x . The optical path of the probe beam thereby changes, and the probe pulse arrival time at the sample is slightly shifted. This is easily compensated in the data analysis for each value of x by calibration of the zero delay time setting using the observed reflectance spike associated with the pump pulse arrival at the sample. The pump and probe beams are merged by a dichroic beam splitter placed in the optical path before the microscope objective. The average powers of the pump and probe beams before the objective lens are 2 and 1 mW, respectively. (This objective transmits $\sim 75\%$ of the light at the corresponding wavelengths.) The spot size of the focused pump light is $\sim 1\ \mu\text{m}$ (intensity full width of half maximum, FWHM), and that of the probe light is $\sim 2\ \mu\text{m}$. These were measured by a knife-edge technique, assuming Gaussian distributions. The probe beam focusing produces a $\sim \pm 10^\circ$ spread in the incident beam angle on the sample. The pulse energy of the pump light at the sample is $\sim 50\ \text{pJ}$, and the estimated maximum instantaneous and steady-state temperature rises in the sample are $\sim 250\ \text{K}$ and $\sim 25\ \text{K}$, respectively [1,2,7]. The reflected probe light is partially reflected at a beam splitter, and is focused onto a photodetector. The probe light intensity change is detected by a lock-in amplifier synchronized to the chopping frequency of the pump beam. An infrared-pass, blue-cut color filter is placed in front of the photodetector to eliminate pump light. The relative reflectance change $\Delta R/R$ is recorded as a function of delay time τ and the incident probe light displacement x . The pump and probe polarizations are linear and elliptical, respectively.

4. Experimental results

Fig. 3 shows data for the probe relative reflectance change $\Delta R/R$ as a function of the incident probe beam displacement on the microscope objective (with 0.2 mm step) and the delay time (with 0.5 ps step): Fig. 3 (a) shows typical time-domain data for $\Delta R/R$ at two incident displacements ($x = 0.06$ and $x = 1.064$ mm), showing Brillouin oscillations at ~ 20 GHz; Fig. 3(b) shows similar spatiotemporal data on a color scale after subtracting a slowly varying background signal arising mainly from the temperature change of the Ti film. The increase in amplitude at ~ 210 ps corresponds to the arrival of the first echo after phonon reflection from the 640 nm Ti film free surface. The Brillouin oscillations arise solely because of acoustic propagation in the silica substrate. On setting y near zero, the displacement x and the angle θ_0 are related as in Eq. (3): $|x| = 0.5, 1.0,$ and 1.5 mm correspond to $|\theta_0| = 9.5^\circ, 18.4^\circ$ and 26.6° , respectively. Because the Brillouin oscillations are generated by the interference of the probe light reflected at the Ti-SiO₂ interface and at the acoustic pulse wavefront, for larger displacements $|x|$ and delay times t , the optical interference contrast decreases with increasing $|x|$ and t , leading to a lower Brillouin oscillation amplitude.

Fig. 4 shows the frequency of the measured Brillouin oscillations (red squares) obtained by temporal Fourier transforms over 1000 ps as a function of x . The solid line obtained by least-squares fitting to the experimental data with Eqs. (2) and (3) using the focal length F and displacement y as variable parameters, and under the assumption that the refractive index n and longitudinal sound velocity v take their literature values $n = 1.45$ (at 820 nm optical wavelength) and $v = 5968\ \text{m s}^{-1}$ [29]. The center position $x = 0$ corresponds to the maximum value of f_B . This position is obtained before the main fitting procedure by use of a symmetric-curve fitting function. The fitted

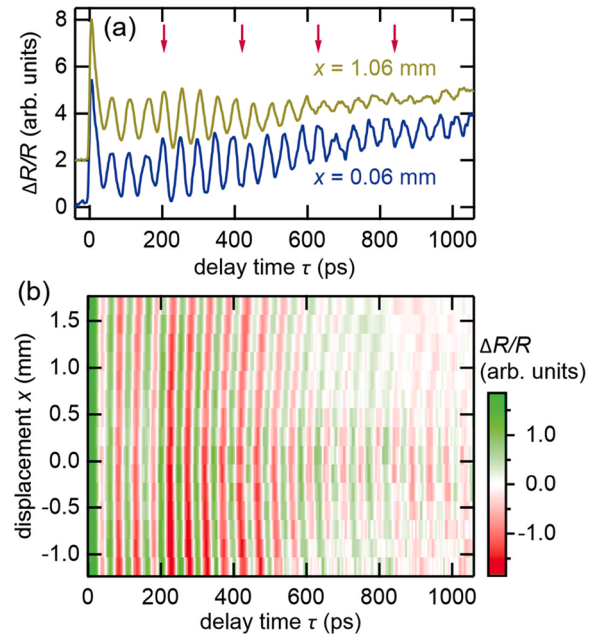


Fig. 3. (a) Probe beam relative reflectance change as a function of delay time τ for some selected lateral displacements x . The downward pointing arrows correspond to the arrival of acoustic echoes. (b) Probe beam relative reflectance change as a function of the probe beam lateral displacement x on the objective lens and the delay time τ . (A slowly varying background signal is subtracted.)

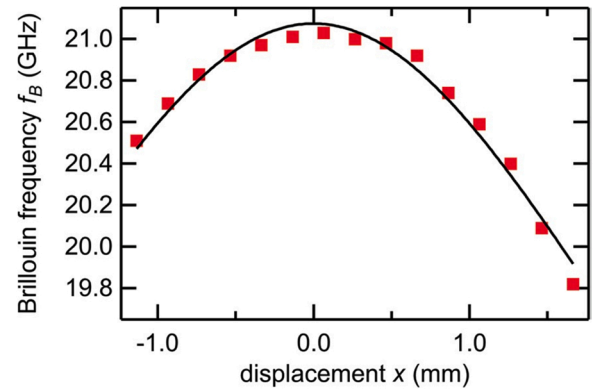


Fig. 4. Frequency of the Brillouin oscillations derived by temporal Fourier transforms of the experimental data (red points) and fitted curve (black solid line) obtained from Eqs. (2) and (3).

average values of F and y are $F = 3.05$ mm and $y = 0.38$ mm. F is very close to the value $F = 3.0$ mm obtained from the datasheet for the objective lens [30] and y is in the expected range determined by alignment. Our results demonstrate that the proposed angle-scanning technique works well over the range $|\theta_0| < 29^\circ$ for the incident angle θ_0 . For measurements on arbitrary samples, initial determination of F and y on a standard sample as presented here should be useful for pre-calibration.

To extract f_B as a function of delay time τ , the TDBS data is further analyzed by the use of STFTs with a Hanning window function $w_H(t) = \frac{1}{2}[1 + \cos(2\pi(t-\tau)/T)]$ for $|\tau-t| \leq T/2$ and $w_H(t) = 0$ for $|\tau-t| > T/2$, where $T = 300$ ps, accommodating about 6 oscillation cycles, is the chosen window duration. By means of temporal Fourier analysis as explained above, the variation of ν and n with τ is obtained from Eqs. (2) and (3) as functions of displacement x and peak Brillouin frequency f_B by means of least-squares fitting to the angle-scanned data for each delay time, while keeping the values $F = 3.05$ mm and $y = 0.38$ mm constant, as shown in Fig. 5(a).

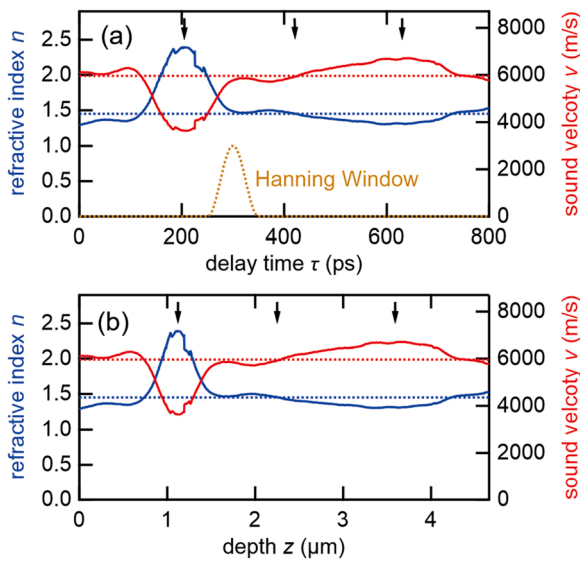


Fig. 5. Derived refractive index (blue solid line) and longitudinal sound velocity (red solid line) in the silica sample as a function of (a) delay time and (b) depth. The dotted lines represent the expected values of refractive index n and longitudinal sound velocity v of silica. Also shown is the Hanning window used (orange dotted line), which is scanned in time to obtain the temporal variation of the Brillouin frequency. The depth profiles in (b) are obtained by use of the measured sound velocity temporal variation in (a). The downward pointing arrows correspond to the arrival of acoustic echoes.

These temporal variations can be converted to spatial variations as a function of the distance (i.e., depth) z from the Ti-SiO₂ interface by integration of the *measured* sound velocity temporal variation, as shown in Fig. 5(b). The derived variations in $n(z)$ and $v(z)$ (solid lines) show good agreement with the expected values (dotted lines) before the arrival of the first echo at ~ 210 ps (when $z \approx 1.2$ μm for the initial pulse) produced by phonon-pulse reflection from the buried Ti-silica interface. Significant deviations in v from the expected value are recorded at this point. The origin of this first echo can be understood as follows. After the short-time thermoelastic stress generation in the Ti film, two counterpropagating phonon pulses of equal amplitude are generated with a strain amplitude $\sim 10^{-3}$ [5]. One part of the upwardly (+ z -directed) propagating phonon pulse is transmitted as a unipolar strain pulse to the silica film and partially reflected at the Ti-silica interface with a strain reflection coefficient of $r = (\rho v - \rho_0 v_0) / (\rho v + \rho_0 v_0) = -0.35$, where literature values of the densities ρ , ρ_0 and longitudinal sound velocities v , v_0 of fused silica and Ti, respectively, are used ($\rho = 2196$ kg m^{-3} and $v = 5968$ m s^{-1} , $\rho_0 = 4510$ kg m^{-3} and $v_0 = 6070$ m s^{-1} [29]). The downwardly ($-z$ -directed) propagating phonon pulse thus shows a bipolar strain profile, and is reflected with a strain reflection coefficient $r_1 = 0.9$ at the Ti-water interface (calculated using the density and sound velocity of water at 20 °C, i.e., 998 kg m^{-3} and 1482 m s^{-1} [29]). After that, it is transmitted at the Ti-silica interface as the first-echo phonon pulse. The calculated ratio of the peak-to-peak strain amplitudes of the first-echo to the initial phonon pulse takes the approximate value 1.2, ignoring negligible ultrasonic attenuation. Subsequent echoes are diminished in amplitude by a factor of ~ 0.32 each time. The arrival of the first echo produces a change in the instantaneous Brillouin frequency unrelated to the predicted value of f_B . For depths greater than $z \approx 1.2$ μm , the predicted values of n and v return as expected close to their predicted values. (As explained above, higher order echoes are expected to produce significantly smaller perturbations to f_B , but their effect is presumably responsible for the residual fluctuations in n and v as a function of depth for $z > 1.2$ μm .) The use of a much thinner (or thicker) transducer film would avoid the perturbations in f_B caused by acoustic

echoes, and permit the accurate monitoring of n and v over greater depths. The accuracy of our method in determining n and v at times before perturbations owing to echo arrival (i.e., for $z \lesssim 0.5$ μm) is $\sim 3\%$, determined we believe by laser intensity fluctuations and residual optical-system alignment errors. With system improvements it should be possible to improve significantly on the measurement accuracy. The spatial resolution in the depth direction in our analysis is estimated to be ~ 900 nm ($\sim 3\Lambda$, where $\Lambda = \lambda / (2n \cos \theta) = 270\text{--}290$ nm is the corresponding acoustic wavelength range for our range of θ), approximately equal to the FWHM temporal duration of the chosen Hanning window function of the STFT multiplied by the value of v . (In comparison, the spatial resolution obtainable using a rectangular window function is approximately equal to half the window temporal duration multiplied by v [20].)

The spatial resolution in the depth direction could be improved by the use of shorter probe-beam wavelengths. The lateral spatial resolution is determined by the pump and probe spot sizes, and could thus be improved by the use of tighter focusing. However, a smaller probe spot size also leads to a smaller Brillouin oscillation amplitude because of degraded optical interference conditions, especially for higher incident probe angles. The pump spot size determines the lateral size of the acoustic pulse, which scatters the probe light. When the pump spot size is much smaller than the probe spot size, as in the present experiment, variations in pump spot size do not affect the probe interference conditions. Smaller pump spot sizes may lead to sample damage, or loss of signal if the pump beam power is reduced. The pump and probe spot sizes should in general be determined by a consideration of the trade-offs between the required lateral resolution, maximum measurement depth, and analysis window duration. An analytical approach to this problem is given elsewhere [31–33].

Our chosen angle range is limited to $|\theta_0| < 27^\circ$, because Brillouin oscillations at larger angles decay to a level that makes it difficult to determine f_B up to 1000 ps, i.e., at depths up to 6 μm . If one requires a more accurate velocity and refractive index determination for measurements limited to smaller depths, the angle range in our system can be increased by use of values of $|x|$ up to 3.5 mm, or $|\theta_0| = 50^\circ$. (Recall that the lens aperture diameter is 8 mm and the probe beam FWHM before the objective is ~ 1 mm.) The corresponding range of f_B increases from 19.8–21.0 GHz to 18.0–21.0 GHz. This may still not be sufficient for applications requiring a larger range of f_B , such as in ultrasonic spectroscopy [9,12] or strain-pulse tomography [28], which make use of a prism or hemisphere for larger incident angles.

5. Conclusions

In conclusion, we present a technique in time-domain Brillouin scattering for the depth profiling of both sound velocity and refractive index in a transparent material based on automated optical probe-incidence scanning. This allows incident-angle resolved measurements in a compact system without the need for a cumbersome optical arrangement. The technique is validated with a well-characterized homogeneous glass sample, but it should also be applicable to inhomogeneous transparent samples, such as solids, liquids or mixtures of the two. In the case in which liquids are involved, the transducer film in contact with the liquid can be deposited on a suitable substrate. Perturbations owing to echo arrivals could be avoided by the use of either very thin or very thick transducer layers. Alternatively, one could make use of pump beam illumination from the bottom side of the sample—an effective method for avoiding damage to delicate samples—combined with an impedance-matched transducer film in order to achieve the same result. It should also be possible to map the sound velocity in 3D in inhomogeneous samples, such as biological cells or inorganic layers with gradients, giving access to micron and sub-micron scale 3D maps of elastic constant variations.

Declaration of Competing Interest

The authors declare the following financial interests/personal relationships which may be considered as potential competing interests: Motonobu Tomoda reports financial support was provided by Japan Society for the Promotion of Science. Osamu Matsuda reports financial support was provided by Japan Society for the Promotion of Science. Oliver B. Wright reports financial support was provided by Japan Society for the Promotion of Science.

Data Availability

Data will be made available on request.

Acknowledgement

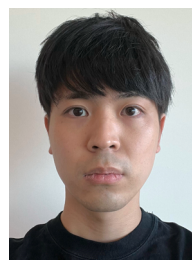
We acknowledge Grants-in-Aid for Scientific Research from the Japan Society for the Promotion of Science.

References

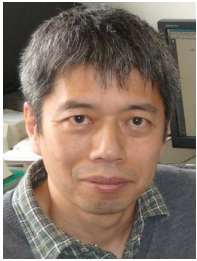
- [1] C. Thomsen, H.T. Grahn, H.J. Maris, J. Tauc, Surface generation and detection of phonons by picosecond light pulses, *Phys. Rev. B* 34 (1986) 4129–4138.
- [2] O. Matsuda, M.C. Larciprete, R.L. Voti, O.B. Wright, Fundamentals of picosecond laser ultrasonics, *Ultrasonics* 56 (2015) 3–20.
- [3] T. Tachizaki, T. Muroya, O. Matsuda, Y. Sugawara, D.H. Hurley, O.B. Wright, Scanning ultrafast Sagnac interferometry for imaging two-dimensional surface wave propagation, *Rev. Sci. Instrum.* 77 (2006), 043713.
- [4] H.-N. Lin, R.J. Stoner, H.J. Maris, J. Tauc, Phonon attenuation and velocity measurements in transparent materials by picosecond acoustic interferometry, *J. Appl. Phys.* 69 (1991) 3816–3822.
- [5] O.B. Wright, T. Hyoguchi, Ultrafast vibration and laser acoustics in thin transparent films, *Opt. Lett.* 16 (1991) 1529–1531.
- [6] O. Wright, Laser picosecond acoustics in double-layer transparent films, *Opt. Lett.* 20 (1995) 632–634.
- [7] S. Kashiwada, O. Matsuda, J.J. Baumberg, R.L. Voti, O.B. Wright, In situ monitoring of the growth of ice films by laser picosecond acoustics, *J. Appl. Phys.* 100 (2006), 073506.
- [8] C. Rossignol, N. Chigarev, M. Ducouso, B. Audoin, G. Forget, F. Guillemot, M. C. Durrieu, In vitro picosecond ultrasonic in a single cell, *Appl. Phys. Lett.* 93 (2008), 123901.
- [9] T. Pezeril, C. Klieber, S. Andrieu, K.A. Nelson, Optical generation of gigahertz-frequency shear acoustic waves in liquid glycerol, *Phys. Rev. Lett.* 102 (2009), 107402.
- [10] B. Audoin, C. Rossignol, N. Chigarev, M. Ducouso, G. Forget, F. Guillemot, M. C. Durrieu, Picosecond acoustics in vegetal cells: non-invasive in vitro measurements at a sub-cell scale, *Ultrasonics* 50 (2010) 202–207.
- [11] A.M. Lomonosov, A. Ayouch, P. Ruello, G. Vaudel, M.R. Baklanov, P. Verdonck, L. Zhao, V.E. Gusev, Nanoscale noncontact subsurface investigations of mechanical and optical properties of nanoporous low-k material thin film, *ACS Nano* 6 (2012) 1410–1415.
- [12] C. Klieber, T. Pezeril, S. Andrieu, K.A. Nelson, Optical generation and detection of gigahertz-frequency longitudinal and shear acoustic waves in liquids: theory and experiment, *J. Appl. Phys.* 112 (2012), 013502.
- [13] S.M. Nikitin, N. Chigarev, V. Tourmat, A. Bulou, D. Gasteau, B. Castagnede, A. Zerr, V.E. Gusev, Revealing sub- μm and μm -scale textures in H_2O ice at megabar pressures by time-domain Brillouin scattering, *Sci. Rep.* 5 (2015) 09352.
- [14] T. Dehoux, K. Ishikawa, P.H. Otsuka, M. Tomoda, O. Matsuda, M. Fujiwara, S. Takeuchi, I.A. Veres, V.E. Gusev, O.B. Wright, Optical tracking of picosecond coherent phonon pulse focusing inside a sub-micron object, *Light Sci. Appl.* 5 (2016), e16082.
- [15] O. Matsuda, T. Pezeril, I. Chaban, K. Fujita, V. Gusev, Time-domain Brillouin scattering assisted by diffraction gratings, *Phys. Rev. B* 97 (2018), 064301.
- [16] O. Matsuda, K. Tsutsui, G. Vaudel, T. Pezeril, K. Fujita, V. Gusev, Optical generation and detection of gigahertz shear acoustic waves in solids assisted by a metallic diffraction grating, *Phys. Rev. B* 101 (2020), 224307.
- [17] C. Mechri, P. Ruello, J.M. Breteau, M.R. Baklanov, P. Verdonck, V. Gusev, Depth-profiling of elastic inhomogeneities in transparent nanoporous low-k materials by picosecond ultrasonic interferometry, *Appl. Phys. Lett.* 95 (2009), 091907.
- [18] V. Gusev, A. Lomonosov, P. Ruello, A. Ayouch, G. Vaudel, Depth-profiling of elastic and optical inhomogeneities in transparent materials by picosecond ultrasonic interferometry: theory, *J. Appl. Phys.* 110 (2011), 124908.
- [19] S. Danworaphong, M. Tomoda, Y. Matsumoto, O. Matsuda, T. Ohashi, H. Watanabe, M. Nagayama, K. Gohara, P.H. Otsuka, O.B. Wright, Three-dimensional imaging of biological cells with picosecond ultrasonics, *Appl. Phys. Lett.* 106 (2015), 163701.
- [20] F. Pérez-Cota, R.J. Smith, E. Moradi, L. Marques, K.F. Webb, M. Clark, High resolution 3D imaging of living cells with sub-optical wavelength phonons, *Sci. Rep.* 6 (2016) 1–11.
- [21] M.A. Ghanem, T. Dehoux, L. Liu, G.L. Saux, L. Plawinski, M.-C. Durrieu, B. Audoin, Opto-acoustic microscopy reveals adhesion mechanics of single cells, *Rev. Sci. Instrum.* 89 (2018), 014901.
- [22] F. Pérez-Cota, R. Fuentes-Domínguez, S.L. Cavera, W. Hardiman, M. Yao, K. Setchfield, E. Moradi, S. Naznin, A. Wright, K.F. Webb, A. Huett, C. Frie, V. Sotile, H.M. Elsheikha, R.J. Smith, M. Clark, Picosecond ultrasonics for elasticity-based imaging and characterization of biological cells, *J. Appl. Phys.* 128 (2020), 160902.
- [23] S. La Cavera, F. Pérez-Cota, R.J. Smith, M. Clark, Phonon imaging in 3D with a fibre probe, *Light Sci. Appl.* 10 (2021) 1–13.
- [24] V.E. Gusev, P. Ruello, Advances in applications of time-domain Brillouin scattering for nanoscale imaging, *Appl. Phys. Rev.* 5 (2018), 031101.
- [25] T. Thréard, E. de Lima Savi, S. Avanesyan, N. Chigarev, Z. Hua, V. Tourmat, V. E. Gusev, D.H. Hurley, S. Raetz, Photoacoustic 3D imaging of polycrystalline microstructure improved with transverse acoustic waves, *Photoacoustics* 23 (2021), 100286.
- [26] S. Sandeep, T. Thréard, E. de Lima Savi, N. Chigarev, A. Bulou, V. Tourmat, A. Zerr, V.E. Gusev, S. Raetz, 3d characterization of individual grains of coexisting high-pressure H_2O ice phases by time-domain Brillouin scattering, *J. Appl. Phys.* 130 (2021), 053104.
- [27] R. Côte, A. Devos, Refractive index, sound velocity and thickness of thin transparent films from multiple angles picosecond ultrasonics, *Rev. Sci. Instrum.* 76 (2005), 053906.
- [28] M. Tomoda, O. Matsuda, O.B. Wright, Tomographic reconstruction of picosecond acoustic strain propagation, *Appl. Phys. Lett.* 90 (2007), 041114.
- [29] D.R. Lide, CRC Handbook of Chemistry and Physics, 85th edition, CRC Press, Boca Raton, Fla, 2004.
- [30] Data Sheet LUMPLFN60XW and The Concept of Magnification. ([https://www.olympus-lifescience.com/en/pdf/en/pdf-export/objectives/?0\[DIRECTORY::DirFrontend\]\[itemId\]=511706541](https://www.olympus-lifescience.com/en/pdf/en/pdf-export/objectives/?0[DIRECTORY::DirFrontend][itemId]=511706541)), (<https://www.olympus-lifescience.com/en/microscope-resource/primer/anatomy/magnification/>).
- [31] V.E. Gusev, Contra-intuitive features of time-domain Brillouin scattering in collinear paraxial sound and light beams, *Photoacoustics* 20 (2020), 100205.
- [32] V.E. Gusev, T. Thréard, D.H. Hurley, S. Raetz, Theory of time-domain Brillouin scattering for probe light and acoustic beams propagating at an arbitrary relative angle: application to acousto-optic interaction near material interfaces, *arXiv Prepr. arXiv* (2021) (2107.05294).
- [33] M. Tomoda, A. Toda, O. Matsuda, V.E. Gusev, O.B. Wright, Sound velocity mapping from GHz Brillouin oscillations in transparent materials by optical incidence from the side of the sample, *Photoacoustics* 30 (2023), 100459.



Motonobu Tomoda received his Ph.D. degree in engineering at Hokkaido University, Sapporo, Hokkaido, Japan, in 2008. Since 2022, he has been working as an instructor (until 2007) and an assistant professor (from 2007) in the Faculty of Engineering, Hokkaido University. He specializes in picosecond laser ultrasonics in nanostructures, local probing techniques involving ultrasonics and optics, surface acoustic wave imaging, phononic crystals, and acoustic/mechanical metamaterials.



Akihisa Kubota received his B.A. degree in engineering in 2016 and his master's degree in 2018 from Hokkaido University, Sapporo, Hokkaido, Japan. His research interests include laser picosecond ultrasonics.



Osamu Matsuda received his Ph.D. degree in physics at Osaka University, Japan in 1991. He is currently a professor at Hokkaido University, Japan. His research interests include ultrafast spectroscopy, picosecond laser ultrasonics, acoustic wave imaging, phononic crystals, and phononic metamaterials.



Oliver B. Wright has been a Professor at Hokkaido University, Japan since 1996 and a Guest Professor at Osaka University, Japan since 2022. He received his BA in physics at the University of Oxford and his Ph.D. in physics from the University of Cambridge. His current research interests include picosecond laser ultrasonics, acoustic wave imaging, and acoustic metamaterials.



Yoshihiro Sugawara has been a senior researcher at FUJIFILM Corporation, Japan. He received Ph.D. degree in engineering at Hokkaido University, Japan, in 2002. Since 2003, he had been a postdoctoral research fellow in Southampton University, UK, until 2006. He specializes in picosecond laser ultrasonics, surface acoustic wave imaging, plasmonics and acoustic metamaterials.